Title	**CO observations of candidates for carbon-rich asymptotic giant branch and post-asymptotic giant branch stars**
Author(s)	**Volk, K; Kwok, S; Woodsworth, AW**
Citation	**The Astrophysical Journal, 1993, v. 402 n. 1, p. 292-302**
Issued Date	**1993**
URL	**http://hdl.handle.net/10722/179677**
Rights	**Creative Commons: Attribution 3.0 Hong Kong License**

CO OBSERVATIONS OF CANDIDATES FOR CARBON-RICH ASYMPTOTIC GIANT BRANCH AND POST–ASYMPTOTIC GIANT BRANCH STARS

KEVIN VOLK AND SUN KWOK

Department of Physics and Astronomy, The University of Calgary, Calgary, Alberta, Canada T2N 1N4

AND

ANDREW W. WOODSWORTH

Dominion Astrophysical Observatory, National Research Council, 5071 West Saanich Road, Victoria, BC, Canada V8X 4M6

ABSTRACT

Circumstellar CO emission has been detected in a number of featureless or weak SiC emission, low color temperature *IRAS* sources. The CO detections confirm the suggestion that these are either extreme carbon stars, carbon-rich proto–planetary nebulae (PPNs), or carbon-rich planetary nebulae (PNs). We find that the CO emission is relatively stronger for a given luminosity in post-AGB stars than AGB stars, suggesting a more efficient excitation mechanism is at work in the post–AGB phase. One probable post–AGB star was detected in HCN for the first time. The available HCN data suggest a rapid decline in HCN emission after the AGB. Molecular emission is shown to be a useful tracer of the evolution from asymptotic giant branch to the planetary nebula phase.

Subject headings: circumstellar matter — infrared: stars — stars: carbon — stars: post–asymptotic giant branch

1. INTRODUCTION

Stars on the asymptotic giant branch (AGB) can generally be separated into two classes: oxygen-rich (M stars) or carbon-rich (C stars) based on the oxygen to carbon abundance ratio. Some AGB stars have C:O abundance ratios close to 1 and are spectroscopically classified as S stars. It is traditionally assumed that S stars are in transition from M to C stars, but this hypothesis is never demonstrated observationally or theoretically. It is, however, firmly established that stars on the AGB begin as O-rich, and some (probably not all) later develop into C stars as the result of carbon dredge-up from the core (Iben & Renzini 1983). As stars ascend the AGB, they develop increasingly strong stellar winds. Most evolved AGB stars are heavily obscured by dust and are discovered as the result of infrared surveys. The AFGL survey covered the mid-infrared region and discovered infrared sources with color temperatures as low as 300 K. The *IRAS* survey extended the wavelength coverage to 100 μm and detected sources of much lower temperatures. It is possible that some of these low-temperature sources correspond to stars that have very thick dust shells and are near the end of AGB evolution.

Although the photospheric composition cannot be directly observed for these late AGB stars, their O- or C-rich nature can be determined through the circumstellar dust features. Oxygen-rich stars show the 9.7 μm silicate feature (in emission or absorption), and C-rich stars show the 11.3 μm SiC feature or a featureless continuum (cf. Kwok 1987). The properties of evolved O-rich stars have been extensively studied, for they often show OH maser emission and are known as OH/IR stars (Herman & Habing 1987). The most extreme O-rich stars, meaning those with the highest mass-loss rates and reddest colors, are easily identified by their deep silicate absorption features (Kwok, Hrivnak, & Boreiko 1987).

However, the properties of extreme C-rich stars are less well known. The best studied extreme carbon stars are CW Leo (IRC +10°216) and AFGL 3068. The infrared continua of both objects have low color temperatures, suggesting that they have very thick circumstellar envelopes. CW Leo has a weak SiC feature, probably as the result of self-absorption in the highly optically thick dust envelope. AFGL 3068 shows an almost featureless continuum between 10 and 20 μm. These two examples therefore raise the possibility that the most extreme C-rich stars may have no strong circumstellar dust features and can be identified only by their infrared colors.

A search of extreme carbon stars using the *IRAS* Low-Resolution Spectrometer (LRS) data has recently been performed by Volk, Kwok, & Langill (1992, hereafter Paper I). Thirty-one candidates have been identified with *IRAS* colors similar to CW Leo and AFGL 3068, but which show only a weak SiC feature or no feature at all in the 7–23 μm LRS range. Candidates for which near-infrared photometric data are available show a blackbody-like energy distribution, with color temperatures in the range of 300–450 K. Most of these candidates have no known associations with existing astronomical catalogs other than the AFGL catalog. Their color and spectral similarity to CW Leo and AFGL 3068 suggest that these are probably extreme carbon stars (hereafter referred as group 1).

There also exists another group of infrared sources that are featureless in the mid-infrared, but have color temperatures lower than those of the above group, typically 200 K (hereafter referred to as group 2). The LRS spectra of 12 sources with these properties are plotted in Figure 1. The LRS spectra were extracted and processed at the University of Calgary *IRAS* Data Analysis Facility (cf. Volk et al. 1991). Although the nature of these low color temperature sources is not certain, it is likely that they have evolutionary connections to extreme carbon stars, probably C-rich proto–planetary nebulae (PPNs), or C-rich planetary nebulae (PNs). We have plotted the color distribution of these two groups of C-rich objects in Figure 2. We can see that the two groups are clearly separated in *IRAS* colors.
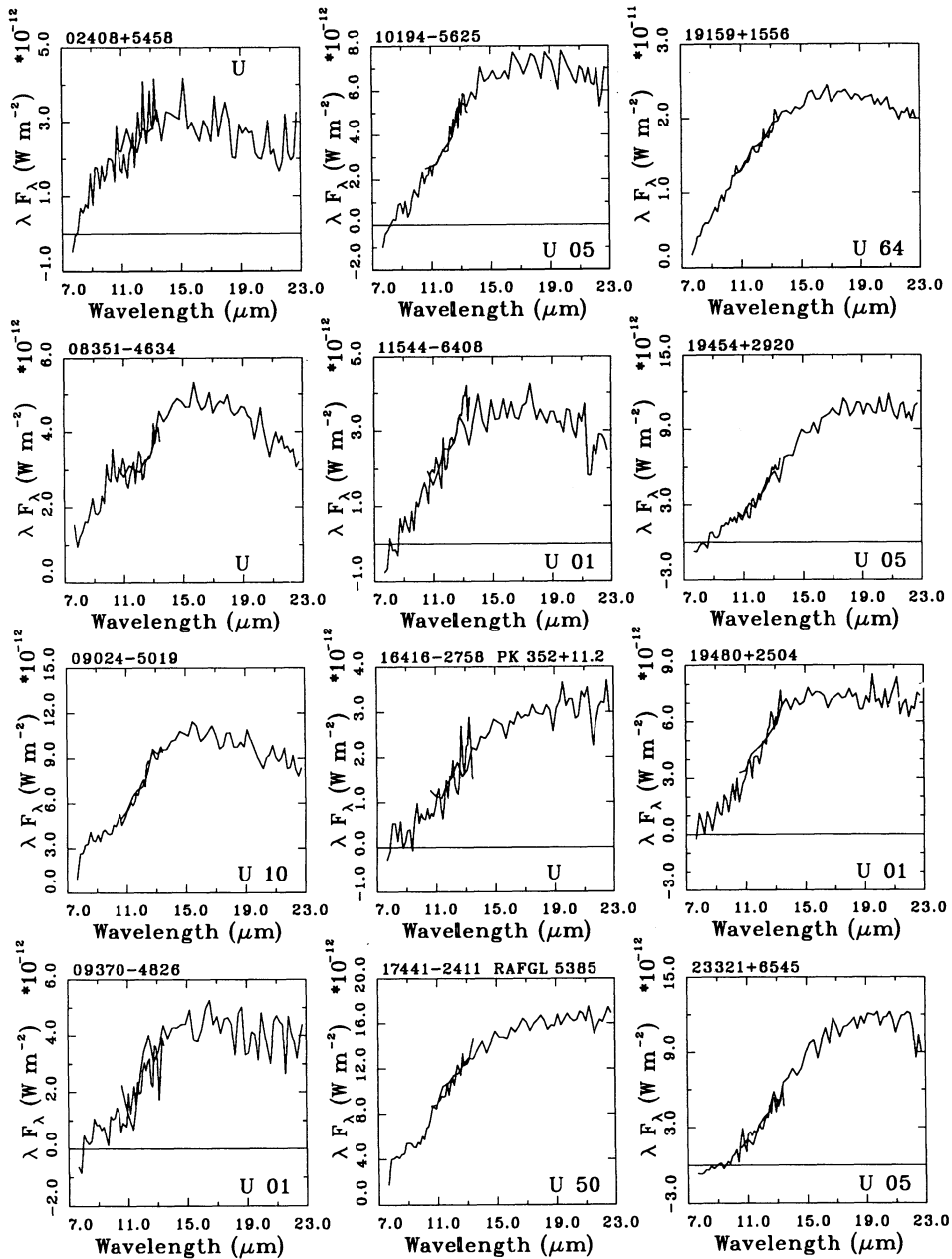
FIG. 1.—The LRS spectra of 12 low color temperature featureless *IRAS* sources. Other catalog associations (when present) are listed next to the *IRAS* names. The letter code U refers to the spectral classification code of Volk & Cohen (1989), and the two-digit spectral classification codes are those of the LRS Atlas.

The nature of the above two groups of low color temperature, featureless continuum objects can only be exactly determined by infrared spectroscopy. However, because of the sharp dropoff in the energy distribution shortward of 10 μm, this is not easy to undertake. While highly evolved C stars do not have the unique signature of OH maser emission as in O-rich stars, they should all show strong optically thick thermal CO emission (Knapp et al. 1982). Highly evolved C stars are expected to have flat tops (resolved) or parabolic (unresolved) profiles and velocity widths of ~ 30 km s^{-1} which distinguish them from CO emissions from interstellar molecular clouds. CO emission from O-rich stars appears to be ~ 3 times weaker than for C stars when other factors are equal (Knapp & Morris 1985). If some of these objects are PPNs or young PNs, CO emission should still be present for the remnant circumstellar envelopes. Of the total of 43 objects in these two groups, 27 are located north of declination $-30°$ and are accessible to a northern millimeter wavelength telescope. In this paper, we report a survey of these two classes of objects in CO and HCN using the James Clerk Maxwell Telescope.

2. OBSERVATIONS

The observations were carried out on the first shifts of the nights of 1991 October 25–27, using the 15 m James Clerk Maxwell Telescope located on Mauna Kea, Hawaii. The telescope beam size at 230 GHz is 22″, which is well suited for stellar observations. The CO observations were carried out under the dual-polarization mode, which reduces the observ-
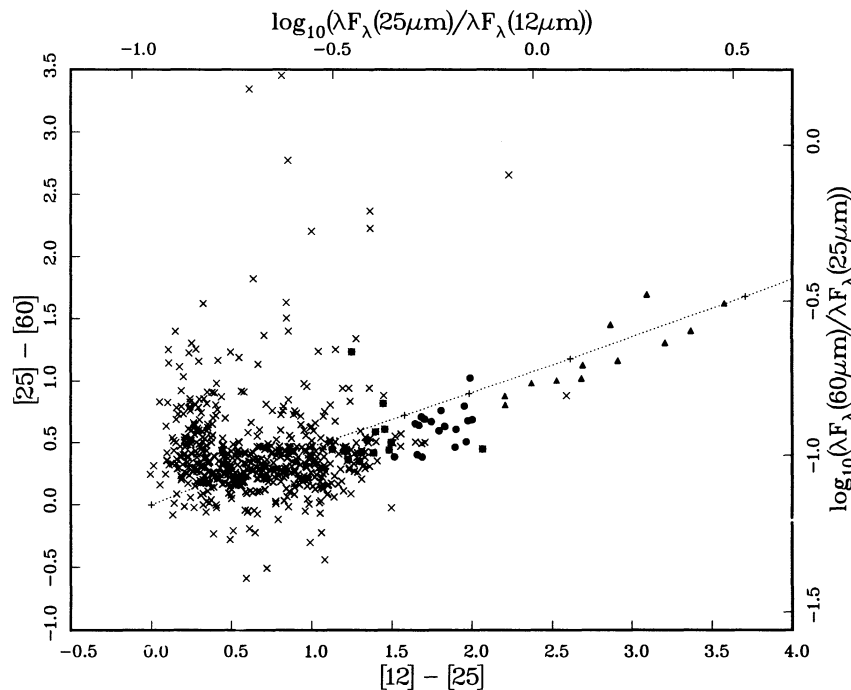
FIG. 2.—Distribution of the group 1 and group 2 carbon-rich objects in the *IRAS* color-color diagram. Group 1 sources are shown as filled circles, and group 2 sources as filled triangles. Also plotted are the 564 stars (*crosses*) in the LRS Atlas that are classified as group C (11.3 μm emission; cf. Volk et al. 1991). The blackbody curve is shown as a dotted line. The *IRAS* colors are as defined by Walker & Cohen (1988).

ing time by a factor of 2 for an unpolarized source. The 2048 channel acousto-optical spectrometer (AOSC) was used for the back end. The channel spacing is 250 KHz, which corresponds to an effective resolution of 330 kHz, or a velocity resolution of 0.44 km s^{-1} at 230 GHz. In the dual-polarization mode, the frequency shift was set to about 1000 channels, so the 2048 spectrometer channels were organized into two 1024 channel spectra. The processing software later averaged the two polarizations, optically scaling them by some factor to account for gain differences in the two IF paths. The CO rest frequency was set at 230.538 GHz.

The observing procedure involving chopping against a cold load, and alternating on- and off-source measurements. The time at each position was generally 60 s. For the spectral observations a chopper beam throw of 3′ in azimuth and a chopping frequency of 1 Hz were used. The typical integration time per source was 40 minutes. The telescope pointing and focus were initially set by observing Uranus and were rechecked several times during the night by observing compact H II regions taken from a list of suitable pointing targets. The changes in pointing were typically 2″–3″, much smaller than the telescope beam-width.

The scans were analyzed at the telescope using the SPECX package to combine the two polarizations of each scan and then to average all the scans for each object. The line widths, peak values, and integrated intensities were found using the SPECX software.

Three of the program sources were also observed in the 265.8864 GHz HCN ($J = 3 \rightarrow 2$) line on October 27. For these higher frequency observations the dual-polarization method could not be used and normal spectral observations were carried out. The typical system temperatures for October 25 and 26 were ∼900 K at 230 GHz. On October 27, the weather

conditions were worse and the system temperature was about 1350 K at 230 GHz and 3000 K at 266 GHz.

The program sources initially included all of the sources from Paper I with R.A. between 19 and 07. Several sources were excluded because they had already been observed (see Zuckerman & Dyck 1986a and references therein) in both CO ($J = 1 \rightarrow 0$) and ($J = 2 \rightarrow 1$). AFGL 3068 was observed for comparison, although it has been well observed in the past. In addition, four group 2 sources with R.A. from 19 to 24 were included in the program. The young, C-rich PN IRAS 21282 + 5050 was also observed for comparison, because some of the extreme carbon star candidates may be evolving towards the PN phase (those with faint optical counterparts; see Paper I) and because the low-temperature sources may be PNs. IRAS 21282 + 5050 was detected in ^{12}CO and ^{13}CO by Likkel et al. (1988). They also detected HCO$^+$ but not H$_2$O, HCN, OH, SO$_2$, or H$_2$S.

3. RESULTS

The results of the observations are shown in Figure 3 for all of the detections plus the HCN nondetection for IRAS 21282 + 5050. In all cases the measured antenna temperature T_A^* is used. The radiation temperature T_r^* can be obtained from T_A^* by dividing by the forward-scattering beam efficiency (η) which we take to be 0.7 at 230 GHz (Matthews 1991). The measured line parameters for all the sources are listed in Table 1. The table gives the line peak T_A^*, the integrated line intensity, the line center LSR velocity (V_{lsr}) and the envelope expansion velocity (V_e). IRAS 19480 + 2504 was only observed for 20 minutes at high airmass, so the quality of the data for this source is poorer than for any of the others. Only two of the sources were not detected in CO: IRAS 19238 + 1159 from the
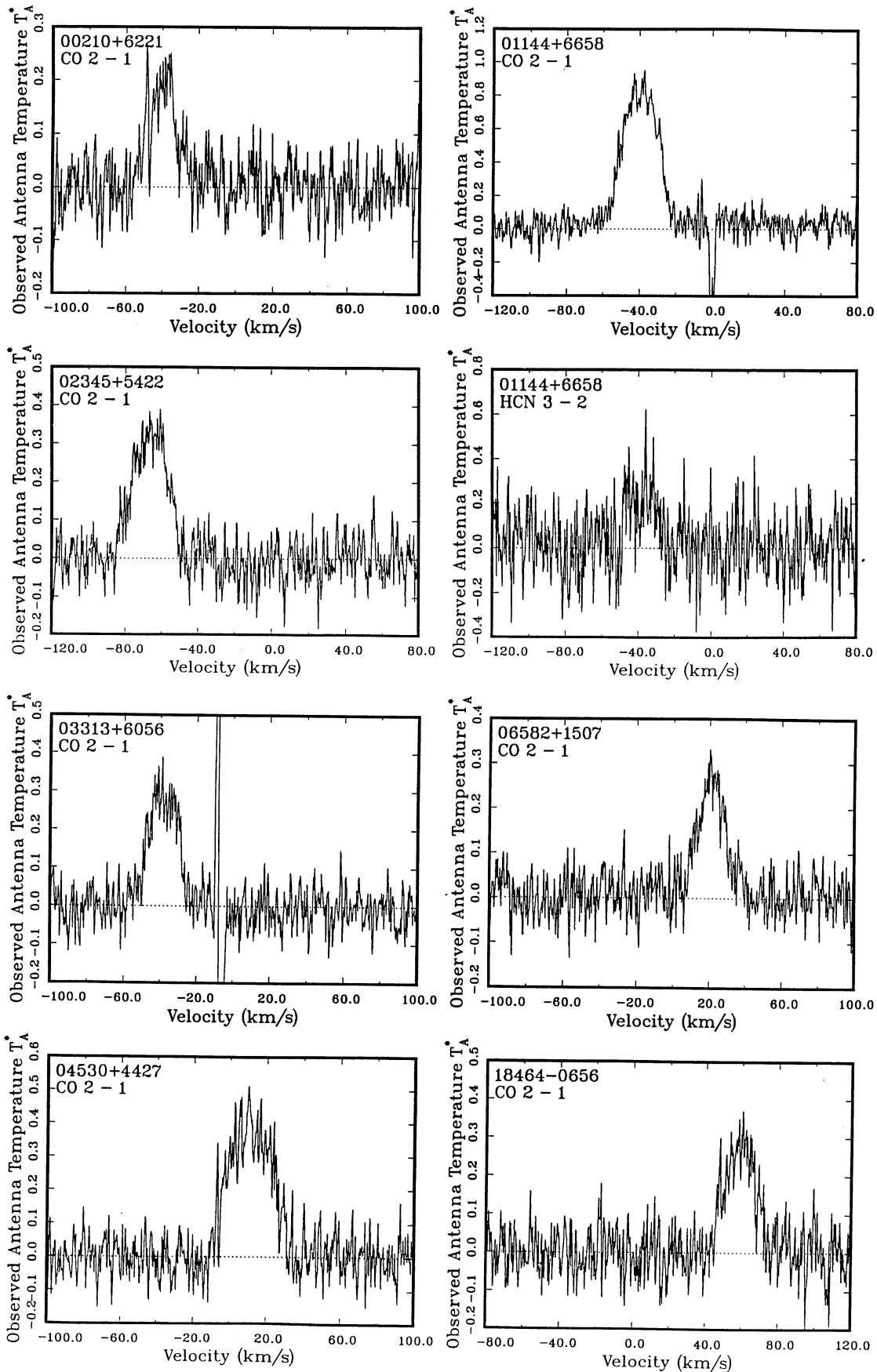
FIG. 3.—The CO (2–1) and HCN (3–2) spectra for the 17 detected sources, plus the nondetection of HCN (3–2) in IRAS 21282+5050, after baseline subtraction and the combining of individual observations with the SPECX software.
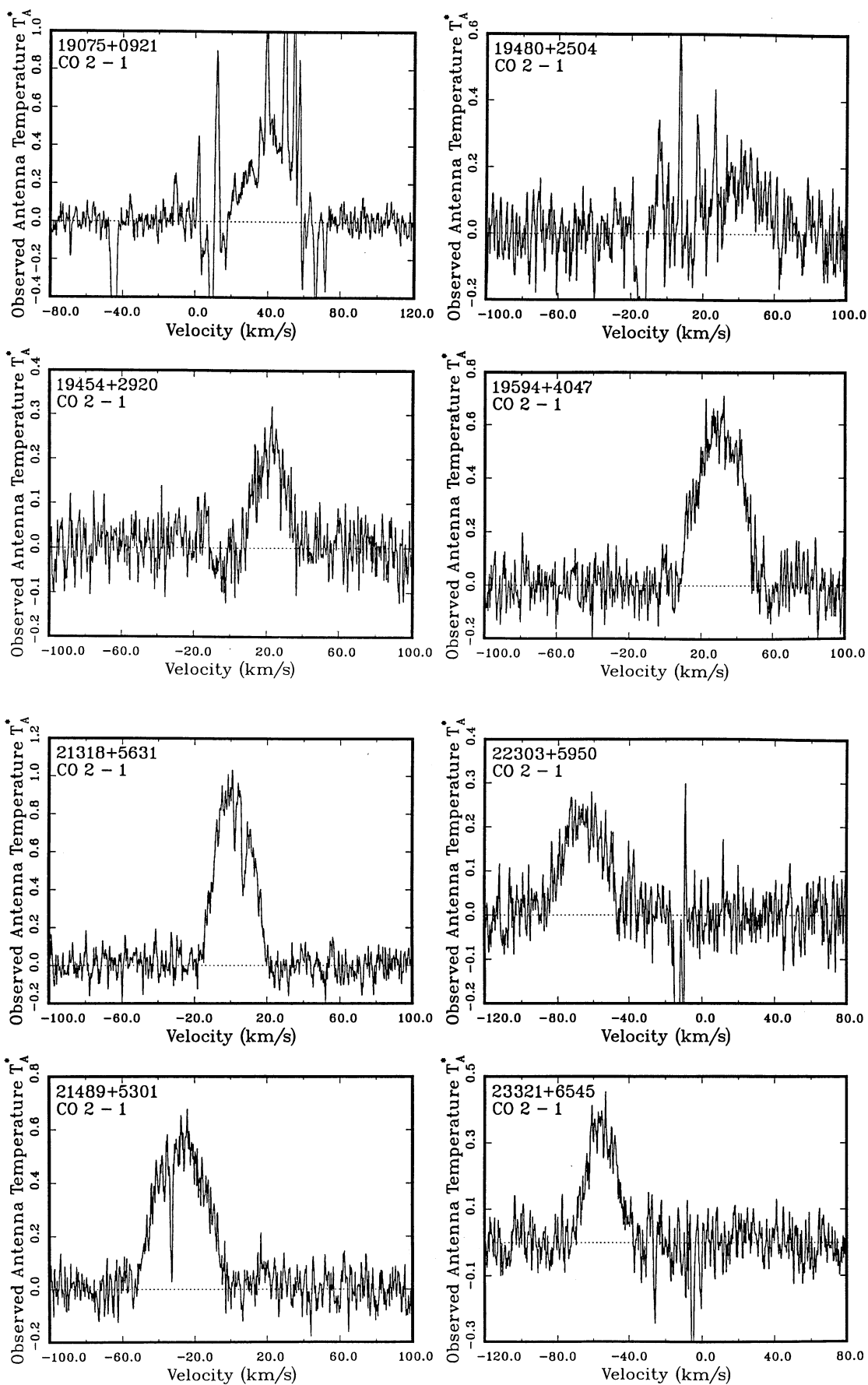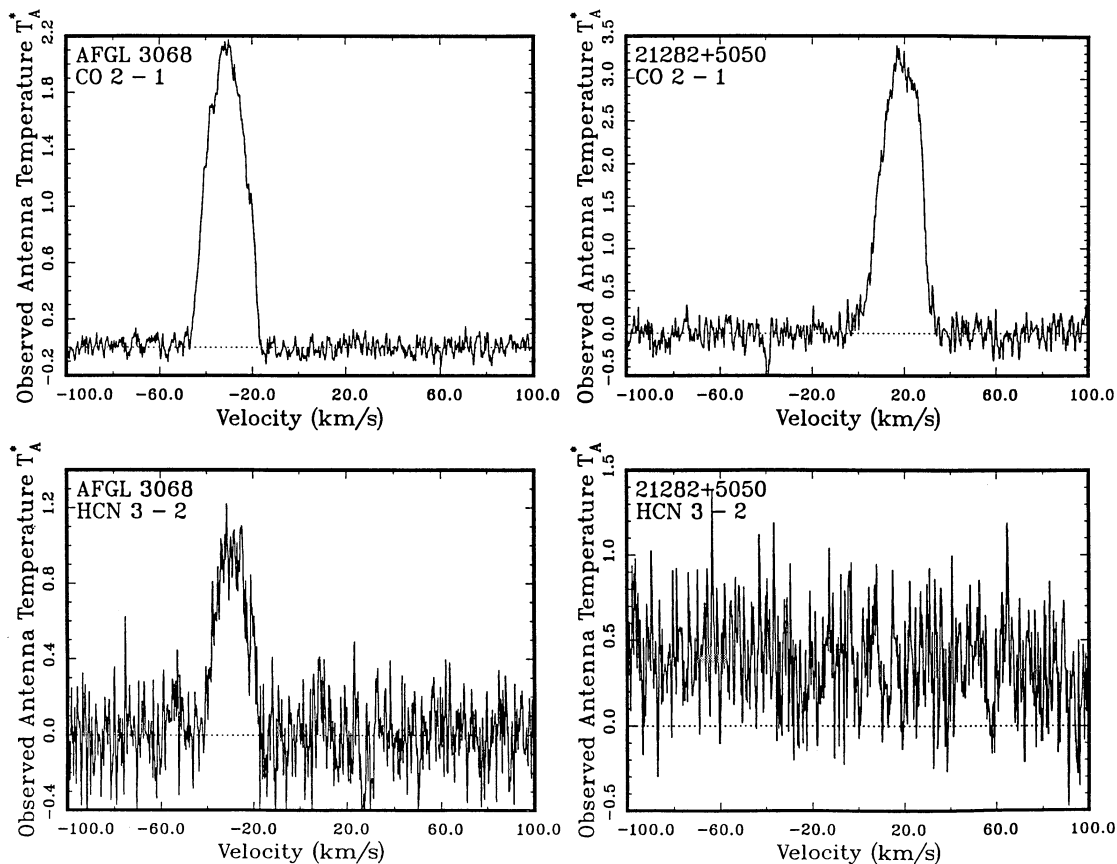
19075+0921
CO 2 − 1

19480+2504
CO 2 − 1

19454+2920
CO 2 − 1

19594+4047
CO 2 − 1

21318+5631
CO 2 − 1

22303+5950
CO 2 − 1

21489+5301
CO 2 − 1

23321+6545
CO 2 − 1

Fig. 3—*Continued*

296

FIG. 3—Continued

TABLE 1

OBSERVED PARAMETERS

| IRAS Name	Line	Peak T_A^* (K)	$\int T_A^* dV$ (K km s^{-1})	V_{LSR} (km s^{-1})	V_e (km s^{-1})
00210+6221............	CO	0.20	3.7	−39.9	16.7
01144+6658............	CO	0.77	19.0	−40.0	19.6
02345+5422............	CO	0.31	7.7	−67.0	19.0
03313+6058............	CO	0.27	5.8	−38.3	13.9
04530+4427............	CO	0.35	11.2	+10.7	20.9
06582+1507............	CO	0.28	5.1	+24.0	16.6
18464−0656............	CO	0.27	5.7	+59.3	16.7
19075+0921............	CO	0.43	16.0	+38.2	21.6
19159+1556............	CO	<0.15	...	...	...
19238+1159............	CO	<0.15	...	...	...
19454+2920............	CO	0.21	3.8	+19.7	17.8
19480+2504............	CO	0.17	5.8	+42.0	27.0
19594+4047............	CO	0.56	17.1	+22.1	19.6
21282+5050............	CO	3.01	65.1	+15.7	19.8
21218+5631............	CO	0.89	20.6	+1.7	19.6
21489+5301............	CO	0.54	17.1	−27.2	26.7
22303+5950............	CO	0.22	6.0	−66.9	20.6
23166+1655............	CO	2.03	40.2	−31.7	15.7
23321+6545............	CO	0.37	7.1	−55.3	18.2
01144+6658............	HCN	0.23	4.6	−37.6	14.2
21282+5050............	HCN	<0.2	...	...	...
23166+1655............	HCN	0.93	16.0	−29.6	12.4

297
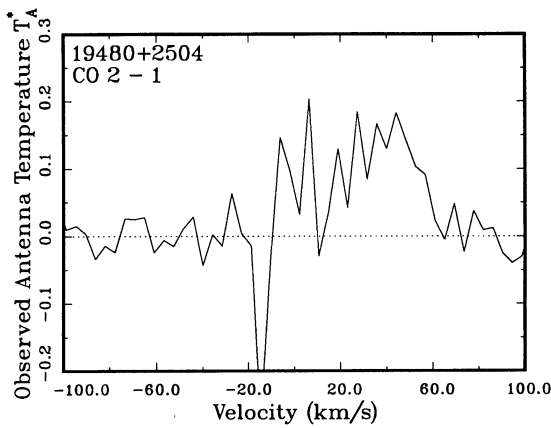
Fig. 4.—The CO spectrum of IRAS 19480+2504 after averaging over 10 channels.

extreme carbon star candidates and IRAS 19159+1556 from the low-temperature sources.

For the two sources for which CO was not detected, the upper limits are estimated from the noise level. For IRAS 19480+2504 the detection is marginal, so we show the spectrum binned over 10 channels in Figure 4. There is some interstellar CO absorption in the reference beam for this source, which causes a distortion of the lower velocity part of the profile. Due to the poorer quality of the spectrum, the derived values for this source are less accurate than for the other sources.

Three of the brightest CO sources (AFGL 3068, IRAS 21282+5050, and IRAS 01144+6658) were also observed in the HCN ($J = 3 \rightarrow 2$) line. The integration time was 30 minutes per source. AFGL 3068 was clearly detected, IRAS 01144+6658 was detected with poor signal-to-noise ratio, and IRAS 21282+5050 was not detected. The nondetection of HCN ($J = 3 \rightarrow 2$) in IRAS 21282+5050 is consistent with the nondetection of HCN ($J = 1 \rightarrow 0$) by Likkel et al. (1988). HCN ($J = 1 \rightarrow 0$) was detected in IRAS 01144+6658 by Zuckerman

& Dyck (1986a), and in AFGL 3068 by Sopka et al. (1989). None of these sources has been previously observed in HCN ($J = 3 \rightarrow 2$).

3.1. Derived Mass-Loss Rates

All of the sources which have been detected have parabolic or flat-topped CO emission profiles. Assuming that the profiles are the result of optically thick envelopes, the mass-loss rates for the stars can be estimated using a formula of Knapp & Morris (1985), corrected for the different beam characteristics of the telescope and for the higher transition as discussed in Woodsworth et al. (1991):

$$\dot{M} = 4.7 \times 10^{-8} (T_A^*/K)(V_e/km\ s^{-1})^2 (D/kpc)^2\ M_\odot\ yr^{-1}$$

where T_A^* is the antenna temperature corrected to outside Earth's atmosphere, V_e is the envelope expansion velocity, and D is the distance. The derived mass-loss rates as a function of distance are given in Table 2. This formula assumes a CO to H_2 abundance ratio of 8×10^{-4}.

Distance estimates to any of these sources are difficult to obtain. Kinematic distances can be found for 11 of the 17 sources in Table 2, but the radial velocities of AFGL 3068 and IRAS 21282+5050, which are probably close by, indicate significant deviations from the Galactic rotation curve so the values are probably not too accurate. The alternative is to assume a constant bolometric or infrared luminosity and derive a distance from the IRAS data, as is done by Jura & Kleinmann (1990). Since the intrinsic luminosities of AGB stars range over a factor of 10, this method can also have large errors. The Jura & Kleinmann (1990) distances are always much smaller than the kinematic distances, often by more than a factor of 2, but even these distances lead to mass-loss rates for 5.4×10^{-6} to 3.5×10^{-4} $M_\odot$ yr^{-1} with most of the values near 2×10^{-5} $M_\odot$ yr^{-1} and only one derived mass-loss rate $< 1 \times 10^{-5}$ $M_\odot$ yr^{-1}. Thus we take 2×10^{-5} $M_\odot$ yr^{-1} to be a typical mass-loss rate for these sources, but this estimate is very uncertain.

For AFGL 3068, IRAS 04530+4427, and IRAS

TABLE 2
DERIVED PARAMETERS

IRAS Name (1)	$\dot{M}/D^{2a}$ ($M_\odot$ yr^{-1}/kpc^2) (2)	Observed Flux[b] (ergs cm^{-2} s^{-1}) (3)	$4\pi F(D/kpc)^2$ (100 $L_\odot$) (4)	β (5)	Nature (6)
00210+6221............	2.6 (−6)	1.7 (−8)	5	4.0	PN
01144+6658............	1.4 (−5)	5.2 (−8)	16	8.5	PPN
02345+5422............	5.3 (−6)	1.2 (−8)	4	12.9	...
03313+6058............	2.5 (−6)	1.1 (−8)	3	5.1	...
04530+4427............	7.2 (−6)	3.3 (−8)	10	7.2	C star?
06582+1507............	2.5 (−6)	1.4 (−8)	4	4.6	...
18464−0656............	3.6 (−6)	3.1 (−8)	10	3.1	...
19075+0921............	9.5 (−6)	4.8 (−8)	15	6.8	...
19454+2920............	3.1 (−6)	2.0 (−8)	6	4.5	PPN
19480+2504............	5.8 (−6)	1.4 (−8)	4	17.9	PPN
19594+4047............	1.0 (−5)	1.4 (−7)	48	2.0	C star
21282+5050............	5.6 (−5)	2.1 (−8)	7	76.6	PN
21318+5631............	1.6 (−5)	1.0 (−7)	29	5.5	...
21489+5301............	1.8 (−5)	4.2 (−8)	13	19.0	C star?
22303+5950............	4.4 (−6)	2.2 (−8)	6	7.6	...
23166+1655............	2.4 (−5)	2.6 (−7)	77	2.4	C star
23321+6545............	5.8 (−6)	1.2 (−8)	6	9.0	PPN

[a] The mass-loss rates (col. [2]) are derived from the formula of Knapp & Morris 1985 which may not be applicable to PPNs and PNs.

[b] See § 5.

06582 + 1507 mass-loss rates have been estimated from a dust-continuum radiative-transfer model fit to the observed energy distribution (see Paper I). These mass-loss values scale differently with distance than do the CO estimates, so in principle a distance can be derived by requiring agreement between the two values. However, the model fits in Paper I for all three of these sources indicate a mass-loss rate that is increasing with time. Since the CO mass-loss rates are based on a constant mass-loss assumption, one would expect discrepancies between the mass-loss rates calculated by the two different methods.

From the dust continuum models, we obtain $\dot{M}/D$ of 3.3×10^{-6}, and 2.3×10^{-5} $M_\odot$ yr^{-1} kpc^{-1} for AFGL 3068, IRAS 04530+4427, and IRAS 06582+1507, respectively. Comparison of these values with those in Table 2 suggests that for AFGL 3068 the two estimates are similar and would agree if D is 1.4 kpc. For IRAS 06582+1507 the values are quite different and agreement would require a distance of 9.3 kpc. In both cases the distances found this way are almost certainly too large: they imply distances from the Galactic plane (z) of 910 pc and 1.4 kpc and luminosities of 18,500 and 40,800 $L_\odot$ for AFGL 3068 and 06582+1507, respectively. If the mass-loss rates are not constant, then it is likely that all of the mass-loss rates estimated in Table 2 are systematically underestimated due to the inappropriateness of the Knapp & Morris formula.

IRAS 04530+4427 is an exception to the above statement because the dust mass-loss rate is lower than the CO mass-loss rate. For the two estimates to agree, a distance of about 500 pc is required. However, this would result in a total luminosity of only 350 $L_\odot$. It is possible that the grain formation in the circumstellar shell is much less efficient than was assumed in deriving the gas mass-loss rate from the dust shell radiative transfer model in Paper I, as might occur because the C/O abundance ratio is lower for this source than for typical extreme carbon stars. If the actual distance to this source is 2 kpc, the dust-to-gas ratio would have to be a factor of 4 lower than had been assumed in Paper I. There is no allowable kinematic distance for this source, but estimates from the bolometric of infrared flux give a distance of order 2.5 kpc for this source, with large uncertainties.

A study of S-type stars by Jura (1988) suggests that the mean [CO/H$_2$] value for four S-stars is about a factor of 2 lower than the mean value for carbon stars. This may account for about half of the discrepancy, but the dust formation rate must still be less efficient than usual to allow agreement.

4. INDIVIDUAL SOURCES

Some of these sources have previously been suggested as extreme carbon star candidates either due to the lack of LRS spectral features of because of 11.3 μm SiC emission. In most cases there has been no direct observation of the stellar photosphere for conventional spectral classification, except for AFGL 3068 and IRAS 19594+4047 = AFGL 2494 where the underlying carbon star is directly detected with near-infrared spectrophotometry (Merrill & Stein 1976). In the following sections we discuss the previous observations of these sources and some implications of our observations.

4.1. *Featureless or Weak* SiC *Sources with Color Temperatures of 300–450 K (Group 1)*

IRAS 00210+6221.—CO ($J = 1 \rightarrow 0$) emission was detected by Arquilla, Leahy, & Kwok (1987). This object was found to have a bright ($V = 16.5$) optical counterpart and was suggested as a PN (Hrivnak, Kwok, & Boreiko 1985). The mid-infrared

photometry by Kwok et al. (1987) shows a featureless continuum which is consistent with the *IRAS* LRS spectrum extracted later at the University of Calgary *IRAS* Data Analysis Facility. The excess in the visible part of the spectrum (Paper I) is likely to be due to nebular emission, and the object is probably a very young C-rich PN.

IRAS 01144+6658 (AFGL 190).—This source has been observed several times previously in molecular lines. A previous CO ($J = 2 \rightarrow 1$) observation is given by Zuckerman & Dyck (1986a), giving V_{LSR} and V_e values that are nearly identical to those we have observed. HCN ($J = 2 \rightarrow 1$) was marginally detected by Zuckerman & Dyck (1986b). A combination of the ground-based near-infrared photometry and the *IRAS* data shows that its energy distribution is well fitted by a 313 K blackbody (Paper I).

IRAS 02345+5422.—There appear to be no previous infrared or molecular line observations of this source besides the *IRAS* data.

IRAS 03313+6058.—Other than the search for OH maser emission (Galt, Kwok, & Frankow 1989), there do not appear to be any previous observations of this source besides the *IRAS* data.

IRAS 04530+4427.—This source has been classified as an infrared carbon star based on the weak 11.3 μm SiC emission feature in its LRS spectrum. Chan & Kwok (1990) derive a mass-loss rate of 5.8×10^{-6} $M_\odot$ yr^{-1} $(D/\text{kpc})^{-1}$ based on the *IRAS* data. CO observations have been made by Zuckerman & Dyck (1986a, b; $J = 1 \rightarrow 0$), and Woodsworth et al. (1991, $J = 2 \rightarrow 1$). HCN ($J = 1 \rightarrow 0$) observations have been made by Nguyen-Q-Rieu et al. (1987). Infrared photometry of this object was reported in Paper I.

IRAS 06582+1507.—This source has no previous observations beside the *IRAS* survey, an unsuccessful OH maser observation by Lewis, Eder, & Terzian (1990), and the infrared observations from Paper I.

IRAS 18464−0656 (AFGL 2256).—Le Squeren et al. (1992) searched and failed to detect OH emission from this object. There are no other ground-based observations.

IRAS 19075+0921.—This source has no previous observations aside from the *IRAS* data. Our JCMT spectrum (see Fig. 3) is contaminated by several narrow interstellar, lines, including some in the reference beam. The line contamination makes the derived line parameters for this source in Tables 1 and 2 somewhat uncertain. The LRS spectrum for 19075+0921 has what appears to be an interstellar silicate absorption feature superimposed on the carbon star spectrum. From the strength of the 10 μm absorption feature, we estimate an A_v of 3.6 mag, assuming the extinction law of Rieke & Lebofsky (1985). This translates to a distance of ~ 4 kpc. If this source is indeed that far away, its mass-loss rate must be extremely high.

IRAS 19238+1159.—There is no previous observation for this object other than the discovery by *IRAS*. Like 19075+0921, the absorption feature at 10 μm is probably interstellar, suggesting a large distance for this object.

IRAS 19594+4047 (AFGL 2494).—This source is known to be a carbon star from near-infrared spectrophotometry (Merrill & Stein 1976). A mass-loss rate of 1.7×10^{-6} $M_\odot$ yr^{-1} $(D/\text{kpc})^{-1}$ was derived by Chan & Kwok (1990) from the infrared data. It has been observed in CO ($J = 1 \rightarrow 0$) and HCN by Zuckerman & Dyck (1986a, b). Near-infrared photometry by Jones et al. (1990) indicates that this star has a 680^d pulsation period.

IRAS 21318+5631.—This source has near-infrared photometric observations by Gaylard et al. (1989). Previous CO

$(1 \rightarrow 0)$ observations are given by Zuckerman, Dyck, & Claussen (1986) and Lindqvist et al. (1988).

IRAS 21489 + 5301.—This source is known to be an infrared carbon star because of the 11.3 μm SiC feature in its LRS spectrum (Chan & Kwok 1990). The mass-loss rate derived from model fitting to the infrared data is $7.1 \times 10^{-6} M_\odot$ yr^{-1} $(D/\text{kpc})^{-1}$. The object was observed in CO $(2 \rightarrow 1)$ by Zuckerman & Dyck (1986a), and in CO $(1 \rightarrow 0)$ and HCN $(1 \rightarrow 0)$ by Nguyen-Q-Rieu et al. (1987).

IRAS 22303 + 5950.—This source is known to be an extreme carbon star due to the SiC feature in its LRS spectrum. It was observed in CO $(1 \rightarrow 0)$ and HCN $(1 \rightarrow 0)$ by Nguyen-Q-Rieu et al. (1987) but otherwise seems to have no data aside from the *IRAS* observations.

4.2. *Low-Temperature (Group 2) Sources*

IRAS 19454 + 2920.—This is one of the first *IRAS* sources found to possess a low-temperature featureless continuum (Kwok et al. 1987). The dust component is well represented by a 190 K blackbody, but in the near-infrared region it shows an excess of a ~ 3500 K blackbody (Kwok, Hrivnak, & Volk 1990). These properties suggest that 19454 + 2920 is a PPN which recently left the AGB. CO emission was first detected by Arquilla, Leahy, & Kwok (1987), and further observations were also obtained by Likkel et al. (1987, 1991).

IRAS 19480 + 2504.—This source was observed in CO by Likkel et al. (1991). Near-infrared photometry (Kwok, Langill, & Hrivnak 1992) shows excess over the dust continuum, suggesting that this is a PPN.

IRAS 23321 + 6545.—This source was observed in CO by Likkel et al. (1987, 1991). As in the case of 19454 + 2920, they obtained a smaller V_e value than we did. This object was also detected at $\lambda 1.3$ mm by Walmsley et al. (1991).

The CO detection of three of the four sources with low-temperature, featureless *IRAS* LRS spectra indicates that these sources have expanding circumstellar envelopes similar to those of the extreme carbon star candidates. However, it is puzzling that IRAS 19159 + 1556 was not detected. As can be seen from Figure 1, this has the brightest LRS spectrum of the four objects. There is another peculiarity of IRAS 19159 + 1556 compared with the other sources. The *IRAS* broad-band photometry data for this object is badly inconsistent with the LRS spectrum. The measured flux densities for IRAS 19159 + 1556 are 1.92 Jy at 12 μm and 1.08 Jy at 25 μm. For comparison, the values for IRAS 23321 + 6545 are 13.66 Jy at 12 μm and 85.61 Jy at 25 μm. If one assumes that the 25 μm flux density and the LRS flux density near 23 μm should be proportional for these two objects, since their spectral shapes are very similar, the resulting estimated 25 μm flux density for IRAS 19159 + 1556 is 143 Jy, or more than 100 times larger than the observed value. The discrepancy at 12 μm is also quite large.

Such a disagreement between the LRS data and the photometric data is very unusual. The LRS had an instantaneous field of view that was 6' by 15', compared with about 0.5 square for the photometric observations at 12 and 25 μm. If the source is significantly extended this might explain the brightness disagreement, for this is occasionally observed in other cases where the source is known to be more extended than the size of the *IRAS* photometric beam, but there was no hint that the source is extended in the photometric observations. The data scans matched the point-source template very well at 12 and 25 μm according to the *IRAS* Point Source Catalog, nor do the LRS data scans show any unusual features, as would be expected if the source were of similar size to the LRS aperture.

In order to resolve these questions, we sent a query to IPAC to check the source for evidence of extendedness. There are indications in the survey scans that 19159 + 1556 was confused with a near-field source, probably an asteroid. This would explain the flux density discrepancy and the lack of CO emission in the object.

The three detected group 2 sources do not seem to show a correlation between the CO line strength and the *IRAS* photometry values, or between the derived $\dot{M}/D^2$ values and the *IRAS* photometry values. These three sources are all brighter than IRAS 21282 + 5050 at 25, 60, and 100 μm (the 12 μm flux density from IRAS 21282 + 5050 is strongly affected by the unidentified infrared emission features which seem to produce almost all of the flux at wavelengths shorter than 18 μm) but have much weaker CO emission. However, these sources appear to have a larger CO emission to infrared luminosity ratio than do the extreme carbon star candidates. We will further address this point in § 5.

The referee suggests that the nondetected objects could be OH/IR stars. We consider this unlikely because (*a*) the *IRAS* spectra and colors of these objects are quite different from OH/IR stars and (*b*) OH emission has been searched for but not found in 19238 + 1159 and in three of the four group 2 sources (Lewis et al. 1990; Likkel 1989).

4.3. *The Carbon-rich PN IRAS 21282 + 5050*

For comparison, we have also observed the recently discovered C-rich PN IRAS 21282 + 5050. This object shows PAH features in both the near- and mid-infrared (de Muizon et al. 1986) and is found to have an emission-line spectrum similar to that of PN. From the nebular spectrum, the central star is classified as 07(f)–[WC 11] (Cohen & Jones 1987). It is likely that the featureless dust component represents the remnant of the circumstellar envelope of an extreme carbon star, and the PAH features are excited by the central star which has recently become hot enough to ionize the circumstellar envelope.

CO emission from 21282 + 5050 was detected by Likkel et al (1988). Our CO results for IRAS 21282 + 5050 are not totally in agreement with the previous results of Likkel et al. (1991). In ^{12}CO (2–1) they report a maximum brightness temperature of 15.1 K, $V_{\text{LSR}} = 18.8$ km s^{-1} and $V_e = 15.8$ km s^{-1}. Our V_{LSR} value of $+ 15.7$ differs slightly from their value of 18.8 km s^{-1}, but our velocity resolution is better than theirs so our value is likely more accurate. Also, our V_e value is somewhat higher than their value. Their Figure 1 shows the observed CO profiles, which look very similar to the profile we obtained, so the disagreement in V_e is probably due to the use of line profile fits by Likkel et al. (1988). They consider there to be "high-velocity wings" on the CO profile, although their Figure 1 seems to show these wings as extending only of order 5 km s^{-1} beyond the main line component. Their brightness temperature value and our brightness temperature value are consistent if the CO emission has a size of 11", resulting in a factor of 4 greater beam dilution for the JCMT observations compared to IRAM which has a diameter twice that of JCMT.

The mass-loss rate deduced from the CO observations of Likkel et al. (1988) is $1.4 \times 10^{-5} M_\odot$ yr^{-1} $(D/\text{kpc})^2$, which is lower than our value by a factor of 3.7. Even if we adopt their value of V_e, the above rates still differ by a factor of 2.

21282 + 5050 also has an energy distribution which is very unusual for a PN (Kwok et al. 1982). Most of the energy is emitted from the dust component. Based on the analysis of Zhang & Kwok (1991), the fraction of energy emitted by the

dust component is no more than 50% even for very young PN. The properties of 21292 + 5050 can only be understood if it has a massive nucleus ($>1\ M_\odot$) which allows it to evolve across the H-R diagram before the dust envelope dissipates. In this regard, it is very similar to NGC 7027.

Optical and radio imaging of 21292 + 5050 show a size of $\sim 5''$ (Kwok et al. 1992; Likkel et al. 1992). The CO-emitting region is resolved by the Nobeyama Millimeter Array, and the CO emission is found to extend over 15'' (Shibata et al. 1989). This suggests that the nebula is ionization bounded.

4.4. HCN Observations

Three sources were observed in the HCN ($J = 3 \to 2$) transition (see Table 1). Both AFGL 3068 and IRAS 01144 + 6658 have previously been observed in the HCN ($2 \to 1$) transition. The HCN ($2 \to 1$) observations gave line brightness temperatures of 0.55 K for AFGL 3068 using a 42'' FWHP beam and 0.07 K for IRAS 01144 + 6658 using a 69'' FWHP beam (Sopka et al. 1989; Zuckerman & Dyck 1986b). Expressed as ratios to the CO ($1 \to 0$) line, the line strengths are 0.34 and 0.13, respectively. The line V_{LSR} and V_e values from these observations are similar to those we derived from the $3 \to 2$ transition. The line ratios for the higher transitions appear to be slightly larger than for the lower transitions. The ratio of HCN ($3 \to 2$) and CO ($2 \to 1$) peak line intensities is 0.46 for AFGL 3068, 0.30 for IRAS 01144 + 6658, and can be crudely estimated as less than 0.05 for IRAS 21282 + 5050. In terms of integrated line intensity the ratios are 0.40 for AFGL 3068 and 0.24 for IRAS 01144 + 6658.

While Jura (1991) has noted an increase of HCN line strengths with the expansion velocities in AGB stars, this correlation does not extend to PPNs and PNs, which generally have higher expansion velocities. As noted above, the HCN line strengths in fact decreases beyond the AGB. The absence of the HCN in 21282 + 5050 can be understood by the fact that the HCN line requires higher excitation and is generally located in the inner parts of the circumstellar envelope. In the case of 21282 + 5050, the inner part of the envelope is already ionized (out to $\sim 5''$), and therefore no HCN can be detected.

However, the very young PN NGC 7027 is known to show HCN ($2 \to 1$) emission at about 5% of the ($1 \to 0$) line strength (Sopka et al. 1989), which makes its HCN emission more than 15 times stronger than for IRAS 21282 + 5050. Both are C-rich PNs as they both show PAH features. NGC 7027 has a much hotter central star (170,000 vs. 30,000 K), but in comparison to 21282 + 5050, its ionized region (10'') is relatively small compared to its molecular envelope (3'). It is clear that NGC 7027 has a smaller dynamical age than 21282 + 5050, and yet its central star is more evolved. The rapid evolution across the H-R diagram suggests that NGC 7027 has a more massive central star than 21282 + 5050.

4.5. Other Comments

IRAS 06582 + 1507.—This source is unusual among the extreme carbon star candidates because its LRS spectrum is well fitted by a pure graphite (or possibility amorphous carbon) dust shell of very high optical depth (see Paper I). Based upon the model fit, if this source has a luminosity of $\sim 7000\ L_\odot$ typical of a normal AGB star of lower mass it must be at a distance of ~ 4 kpc. It shows no unusual CO properties, having a normal ratio of CO line strength to infrared flux density.

IRAS 21489 + 5301.—This source has an anomalously strong CO line for its infrared fluxes. Its line is about a factor of 2 stronger than would be expected from its 60 μm flux density if other sources in the sample are used to define a mean ratio.

5. MOMENTUM AND RADIATIVE FLUXES IN PPNS AND PNS

The momentum flux–to–luminosity ratio, defined as $\beta = \dot{M}V_e c/L_*$, generally has a value near unity of AGB stars. However, for a number of PNs and PPNs β has been found to exceed unity by a large factor (Knapp & Morris 1985; Knapp 1986). This has been interpreted to imply an absolute decrease in luminosity during the evolutionary transition between AGB and PN phases (Knapp 1987, 1989). In Table 2, we have evaluated the values of β for our program objects. The total emitted flux of the objects (given in col. [3] of Table 2) were estimated by fitting the *IRAS* data by a blackbody curve. Since the energy distribution of most of the sources are dominated by the low-temperature dust component, these values should be accurate to within 25%. Since the PN 21282 + 5050 is likely to be ionization bounded (see § 4.3), the leakage of UV flux should be small. We can see that the values of β range from 2 for the carbon star 19594 + 4047 to 77 for the PN 21282 + 5050. The PPNs also have high (> 5) β values.

The change in the value of β by almost two orders of magnitude is difficult to attribute to luminosity change. The luminosity of PPNs and PNs are due to hydrogen shell burning on a electron-degenerate core and should only be dependent on the core mass, which suffers very small change (and certainly does not decrease) during the PPN-PN evolution. The possibility of the large β values in PNs and PPNs as the result of bipolar morphology was considered by Hrivnak & Kwok (1991). Circumstellar disks viewed edge-on could result in an underestimation of the observed flux in the visible part of the spectrum. While this explanation is attractive qualitatively, it is uncertain whether it can explain the quantitative difference. Another possibility is the CO in PNs and PPNs is excited differently than in AGB stars. For example, the dust temperature is lower in PNs and PPNs, which may result in a larger far-infrared flux in the radiative excitation to vibrational states. Another possibility is that the population distribution of the CO molecule in PNs and PPNs concentrates more in the lower rotational states, resulting in higher excitation temperatures of the lower rotational transitions. These two possibilities should be quantitatively evaluated by line transfer models. In either case, the mass-loss rates cannot be derived from the Knapp & Morris formula, which results in a overestimate of the mass loss rate from PPNs and PNs.

6. SUMMARY AND CONCLUSIONS

We have obtained CO ($J = 2 \to 1$) observations of 19 low color temperature *IRAS* sources that show weak SiC emission or featureless continuum in the 8–22 μm range. Except for the source which was later found to be an astroid, circumstellar CO emission was detected in 17 of the remaining 18 sources. Five of the 17 are new detections (never detected in CO before), and an additional four were detected in the $J = 2 \to 1$ transition for the first time. The high detection rate supports the idea that all of these sources are either extreme carbon stars or carbon stars which have recently left the asymptotic giant branch.

Using a formula adapted from Knapp & Morris (1985), the mass-loss rate as a function of distance has been calculated for all of the sources. If the mean source distance is of order 2–3 kpc, which can be crudely estimated from the *IRAS* data

VOLK, KWOK, & WOODSWORTH

assuming a total luminosity appropriate for an AGB star, the mass-loss rates of these objects are $\sim 2 \times 10^{-5} M_\odot$ yr^{-1}

As previously noted by Knapp (1987), we find that ratio of the CO emission strength to photon flux decreases from AGB stars to PPNs to PNs. This ratio (β) changes from ~ 1 for AGB stars to ~ 100 for PNs. This change cannot be the result of luminosity decrease as suggested by Knapp (1987), and the effect of missing some of the observed flux in a bipolar geometry is also unlikely to adequately explain the magnitude of the difference (Hrivnak & Kwok 1991). We believe that this change is the result of increasng radiative excitation of CO as the dust envelope cools in the post-AGB evolution.

HCN ($3 \rightarrow 2$) observations were carried out for three objects: AFGL 3068, IRAS 01144+6658, and IRAS 21282+5050. The HCN ($3 \rightarrow 2$) to CO ($2 \rightarrow 1$) intensity ratio are 0.46, 0.30, and < 0.05 for these three objects. This decreasing trend of HCN to CO ratio is consistent with the evolutionary states of the three sources: late AGB star–PPN–PN. As the density of the envelope decreases as the result of shell detachment, conditions become less and less favorable to the excitation of HCN. When the inner envelope is finally ionized (as in 21282+5050), HCN can no longer be observed. The possibility of using the HCN to CO ratio as a tracer of post-AGB evolution should be tested in more PPN and young PN.

REFERENCES

Arquilla, R., Leahy, D. A., & Kwok, S. 1987, MNRAS, 220, 125
Atlas of Low Resolution IRAS Spectra. 1986, IRAS Science Team, prepared by F. M. Olnon & E. Raimond (A&AS, 65, 607)
Chan, S. J., & Kwok, S. 1990, A&A, 237, 354
Cohen, M., & Jones, B. 1987, ApJ, 321, L151
de Muizon, M., Geballe, T. R., d'Hendecourt, L. B., & Baas, F. 1986, ApJ, 306, L105
Galt, J. A., Kwok, S., & Frankow, J. 1989, AJ, 98, 2182
Gaylard, M. J., West, M. E., Whitelock, P. A., & Cohen, R. J. 1989, MNRAS, 236, 247
Herman, J., & Habing, H. J. 1985, Phys. Rep., 124 (4), 255
Hrivnak, B. J., & Kwok, S. 1991, ApJ, 368, 564
Hrivnak, B. J., Kwok, S., & Boreiko, R. T. 1985, ApJ, 294, L113
Iben, I., & Renzini, A. 1983, ARA&A, 21, 271
Jones, T. J., Bryja, C. O., Gehrz, R. D., Harrison, T. E., Johnson, J. J., Klebe, D. I., & Lawrence, G. F. 1990, ApJS, 74, 785
Jura, M. 1988, ApJS, 66, 33
———. 1991, ApJ, 372, 208
Jura, M., & Kleinmann, S. G. 1990, ApJ, 364, 663
Knapp, G. R. 1986, ApJ, 311, 731
———. 1987, in Late Stages of Stellar Evolution, ed. S. Kwok & S. R. Pottasch (Dordrecht: Reidel), 103
———. 1989, in IAU Symp. 131, Planetary Nebulae, ed. S. Torres-Peimbert (Dordrecht: Kluwer), 381
Knapp, G. R., & Morris, M. 1985, ApJ, 292, 640
Knapp, G. R., Phillips, T. G., Leighton, R. B., Lo, K. Y., Wannier, P. G., Wootten, H. A., & Huggins, P. J. 1982, ApJ, 252, 616
Kwok, S. 1987, Phys. Rep., 156 (3), 111
Kwok, S., Hrivnak, B. J., & Boreiko, R. T. 1987, ApJ, 312, 303
Kwok, S., Hrivnak, B. J., & Volk, K. 1990, in from Miras to Planetary Nebulae: Which Path for Stellar Evolution?, ed. M. O. Mennessier & A. Omont (Gif-sur-Yvette: Editions Frontières), 435

Kwok, S., Langill, P. L., & Hrivnak, B. J. 1992, in preparation
Lawrence, G., Jones T. J., & Gehrz, R. D. 1990, AJ, 99, 1232
Le Sequeren, A. M., Sivagnanam, P., Dennefeld, M., & David, P. 1992, A&A, 254, 133
Lewis, B. M., Eder, J., & Terzian, Y. 1990, ApJ, 362, 634
Likkel, L. 1989, ApJ, 344, 350
Likkel, L., Forveille, T., Omont, A., & Morris, M. 1988, A&A, 198, L1
———. 1991, A&A, 246, 153
Likkel, L., Morris, M., Omont, A., & Forveille, T. 1992, in preparation
Linkel, L., Omont, A., Morris, M., & Forveille, T. 1987, A&A, 173, L11
Lindqvist, M., Nyman, L. A., Olofsson, H., & Winneberg, A. 1988, A&A, 205, L15
Matthews, H. E. 1991, The James Clerk Maxwell Telescope: A Guide For The Prospective User, Royal Observatory, Edinburgh
Merrill, M., & Stein, W. A. 1976, PASP, 88, 874
Nguyen-Q-Rieu, Epchtien, N., Troug-Bach, & Cohen, M. 1987, A&A, 180, 117
Rieke, G. H., & Lebofsky, M. J. 1985, ApJ, 288, 618
Shibata, K. M., Tamura, S., Deguchi, S., Hirano, N., Kameya, O., & Kasuga, T. 1989, ApJ, 345, L55
Sopka, R. T., Olofsson, H., Johnson, L. E. B., Nguyen-Q-Rieu, & Zuckerman, B. 1989, A&A, 210, 78
Volk, K., Kwok, S., & Langill, P. L. 1992, ApJ, 391, 285, (Paper I)
Volk, K., Kwok, S., Stencel, R., & Brugel, E. 1991, ApJS, 77, 607
Walker, H. J., & Cohen, M. 1988, AJ, 95, 1801
Walmsley, C. M., Chini, R., Kreysa, E., Steppe, H., Forveille, T., & Omont, A. 1991, A&A, 246, 555
Woodsworth, A. W., Kwok, S., Chan, S. J., & Murowinski, R. 1991, A&A, 246, 447
Zhang, C. Y., & Kwok, S. 1991, A&A, 250, 179
Zuckerman, B., & Dyck, H. M. 1986a, ApJ, 304, 394
———. 1986b, ApJ, 311, 345
Zuckerman, B., Dyck, H. M., & Claussen, M. J. 1986, ApJ, 304, 401